Influence of surface ligands on the electronic structure of Fe-Pt clusters: A density functional theory study

Thuy T Trinh,[1] Taisuke Ozaki,[2,*] and Shinya Maenosono[1,†]

[1]*School of Materials Science, Japan Advanced Institute of Science and Technology, 1-1 Asahidai, Nomi, Ishikawa 923-1292, Japan*

[2]*Research Center for Integrated Science, Japan Advanced Institute of Science and Technology, 1-1 Asahidai, Nomi, Ishikawa 923-1292, Japan*

(Received 18 October 2010; revised manuscript received 23 December 2010; published 21 March 2011)

The geometrical and electronic structures of a chemically disordered face-centered-cubic- (*fcc*) FePt cluster capped with various organic ligands, including propanoic acid, propylamine, and propanethiol, were investigated by means of density functional theory (DFT) calculations within a generalized gradient approximation (GGA). Detailed analysis of the electronic structure revealed that (1) Fe atoms are the favored adsorption sites of the ligands on the surface of the FePt cluster; however, for propanethiol, adsorption can also occur at Pt sites. (2) The spin magnetic moment of Fe atoms at adsorption sites in the clusters containing adsorbed ligands decreases slightly compared to that in the bare cluster on the adsorption of the ligand, and it does not depend on the length of hydrocarbon chain of the ligand. The decrease in the magnetic moment originates from the interplay between the strong hybridization of the majority *d* states of Fe atoms with majority *p* states of O, N, and S atoms and the electron transfer between the ligands and Fe atoms on the surface of the clusters involving *d*, *p*, and *s* states of the Fe atoms, as well as from the high symmetry of the surface Fe atoms on adsorption of a ligand.

DOI: 10.1103/PhysRevB.83.104413 PACS number(s): 75.75.Lf, 71.15.Mb, 75.20.En, 75.70.Rf

I. INTRODUCTION

Superparamagnetic chemically disordered face-centered cubic- (*fcc*) FePt nanoparticles (NPs) are expected to behave as high-performance nanomagnets for applications in medicine,[1–4] including drug delivery and magnetic resonance imaging (MRI) contrast agents and for the treatment of hyperthermia. This is because of their high magnetocrystalline anisotropy energy and saturation magnetization. However, the materials used most commonly in actual medical applications are superparamagnetic iron oxide (SPIO) NPs whose magnetic properties are inferior to those of *fcc*-FePt NPs.[5] For medical applications, *fcc*-FePt NPs are usually stabilized and functionalized with capping ligands. However, the magnetic properties of *fcc*-FePt NPs are dependent on the properties of the capping ligands. To exploit the intrinsic properties of *fcc*-FePt NPs, it is desirable to understand the influence of surface states on their magnetic properties.

In fact, recent experiments have indicated that *fcc*-FePt NPs exhibit reduced magnetization due to the formation of a nonmagnetic shell (surface dead layer) *via* bond formation of the polar end group of the capping ligands with the *fcc*-FePt NPs.[6,7] We showed experimentally the different influence of various ligands containing carboxyl, amine, or thiol groups on the saturation magnetization of *fcc*-FePt NPs.[7] Furthermore, the binding of oleic acid and oleylamine as well as alkanethiol and mercaptoalkanoic acid ligands to the surface of FePt NPs has been studied by Fourier transform infrared spectroscopy (FT-IR) and high-resolution x-ray photoelectron spectroscopy (XPS).[8,9] In particular, the observation of both υ(COO) and υ(C = O) vibrational modes for as-synthesized FePt coated with oleic acid/oleylamine indicated that oleic acid binds to the FePt NPs in either a monodentate or bidentate fashion, while oleylamine binds to the FePt NPs through electron donation from the nitrogen atom in the NH_2 group.[8] After the coated NPs were exposed to alkanethiol and mercaptoalkanoic acid ligands, it was found that the mercapto end group displaced oleylamine on the Pt atoms and the carboxylic acid end group displaced the oleic acid on the Fe atoms.[9] Preliminary density functional theory (DFT) calculations by Wu *et al*. implied that the surface bonding interactions of oleic acid and oleylamine with FePt NPs take place predominately at surface Fe sites, and some electron density is transferred from oleylamine to surface Fe sites.[6]

In other research, the spin polarization of FePt NPs has been calculated to decrease at the surface of the transition metal on chemisorption of ligands, changing their magnetism.[10–18] For instance, the adsorption of H, CO, or NO on Ni surfaces reduces the magnetic moment of Ni atoms[10–12]; the same observation has been made for sulfur on Fe surfaces[13,14] and for CO and NO on a Pd_3Mn alloy surface.[15] It has also been shown that the adsorption of O atoms on Fe surfaces slightly enhances the magnetic moment of the Fe atoms.[16–18] However, the interaction of the surface ligands with FePt NPs and their influence on magnetism are not completely understood, even from a theoretical point of view.

In this article, we present a theoretical investigation of the interaction between ligands bearing various end groups, including carboxylate, aminate, and thiolate groups and chemically disordered *fcc*-FePt alloy nanoclusters, and the resulting influence of these interactions on the magnetic properties of the *fcc*-FePt clusters by means of first-principle electronic structure calculations. Based on analyses using Mulliken populations and the density of states as well as the difference in charge density, we further clarify that the interactions between the ligands and *fcc*-FePt clusters arise from interplay between charge transfer and hybridization of orbitals.

II. COMPUTATIONAL DETAILS

The electronic structure of the FePt clusters, including the bare FePt cluster and the FePt clusters containing adsorbed ligands, was self-consistently determined under an electronic

temperature of 300 K by means of spin-polarized DFT[19] within the generalized gradient approximation (GGA).[20] Norm-conserving pseudopotentials were used in a separable form with multiple projectors to replace the deep core potential with a shallow potential.[21] Pseudoatomic orbitals (PAOs) centered on atomic sites were used as basis functions. The PAO basis functions, generated by a confinement scheme,[22] were specified by H4.5-*s*2*p*1, C4.5-*s*2*p*2*d*1, N4.5-*s*2*p*2*d*1, O4.5-*s*2*p*2*d*1, S5.5-*s*2*p*2*d*1, Fe5.0-*s*2*p*2*d*1, and Pt7.0-*s*2*p*2*d*1, where, using the example Pt7.0-*s*2*p*2*d*1, Pt is the atomic symbol, 7.0 is the cutoff radius (Bohr) according to the confinement scheme,[22] and *s*2*p*2*d*1 means the employment of two primitive orbitals for each *s* and *p* orbital and one primitive orbital for the *d* orbital. In the electronic structure calculation, real-space grid techniques were used with a cutoff energy of 200 Ry in numerical integrations and in the solution of the Poisson equation using fast Fourier transform (FFT).[23] In addition, the projector expansion method was employed in the calculation of three-center integrals for the deep neutral atom potentials.[24] The geometrical structures investigated were optimized until the maximum force on atoms becomes less than 5×10^{-4} Hartree/Bohr. All of the calculations were performed by an *ab initio* DFT code, OPENMX.[25]

To test the accuracy of the PBE-GGA functional, which is GGA proposed by Perdew, Burke, and Ernzerhof (PBE),[20] and the basis functions and pseudopotentials used for our calculations, the optimization of bulk FePt with an atomic ratio of 1:1 was performed for various phases, including disordered *fcc*-FePt, ordered *fcc*-FePt, and ordered face-centered tetragonal (*fct*)-FePt under periodic boundary conditions. The theoretical results were found to be in reasonable agreement with available experimental data and other calculated results. The theoretically optimized lattice parameter of the disordered *fcc*-FePt crystal of 3.940 Å was slightly larger than the experimental one (3.820 Å)[26] and larger than the other value obtained theoretically (3.75 Å) using the tight-binding linear muffin-tin orbital method combined with the coherent-potential approximation (TB-LMTO-CPA).[27] For the *fct*-FePt crystal, the theoretically optimized lattice parameter $a = 3.992$ Å and axial ratio $c/a = 0.960$ are in good agreement with experimental values ($a = 3.850$ Å, $c/a = 0.964$)[28] and those from a calculation by Müller *et al.* ($a = 3.872$ Å, $c/a = 0.973$) using the projector-augmented wave (PAW) method and GGA.[29]

III. CALCULATION MODEL

The chemically disordered *fcc*-$Fe_{22}Pt_{21}$ nanocluster containing 43 atoms and with a diameter of about 1 nm was constructed from a primitive cell of a chemically disordered *fcc*-FePt crystal using MATERIALS STUDIO.[30] The detailed construction is as follows: The *fcc*-FePt primitive crystal cell of 4 atoms (2 Fe atoms and 2 Pt atoms) was multiplied to create a supercell containing 32 atoms with a random distribution of Fe and Pt atoms and an atomic ratio of 1:1. The 32-atom supercell was replicated to yield a bulk structure, which was then cut to create a spherical cluster containing 43 atoms. The Fe and Pt atoms in the cluster are distributed randomly with a radial distribution, which means the concentration of substituted Fe and Pt itself increases equally in all directions from a central point. The concentration gradient distribution of the atoms was functionalized in exponential form. To investigate the interactions of the ligands with the cluster and their influence on the magnetism, the adsorption of ligands containing various polar end groups, including propanoic acid (CH_3CH_2COOH), propylamine ($CH_3CH_2CH_2NH_2$), and propanethiol ($CH_3CH_2CH_2SH$), onto the cluster were considered. The influence of hydrocarbon chains on the magnetism of the cluster was also studied through the adsorption of ligands with longer hydrocarbon chains, including lauric acid ($C_{11}H_{23}COOH$), dodecylamine ($C_{11}H_{23}CH_2NH_2$), and dodecanethiol ($C_{11}H_{23}CH_2SH$). Only the adsorption of a single ligand molecule on the cluster was studied. As the initial adsorption structure, oxygen, nitrogen, or sulfur atoms of the polar end groups (-COOH, -NH_2, or -SH) of the ligands were added to iron or platinum atoms on the surface of the cluster at distances that ensure an interaction. For instance, for the adsorption of propanoic acid to iron atoms on the surface of the cluster, we considered five configurations: **A**, **B**, **C**, **D**, and **E**. In configurations **A** and **E**, two oxygen atoms bound to two iron atoms *via* the COO bridging mode, with the COOH group for configuration **A** [Fig. 1(a)] or with COO^- due to the elimination of a hydrogen atom for configuration **E** [Fig. 1(e)]. In configurations **C** and **D**, one oxygen atom bearing hydrogen [O^*(H)] binds to one iron atom with the COOH group intact for configuration **C** [Fig. 1(c)] or with COO^- for configuration **D** [Fig. 1(d)]. In configuration **B**, one oxygen atom lacking hydrogen [O^{**}] binds to one iron atom with the COOH group intact [Fig. 1(b)]. Using this method, all suitable configurations for the shorter hydrocarbon chain ligands were investigated; some are shown in Figs. 1(a)–1(m). Configurations **A**-**F**, **G**-**I,** and **J**-**M** are representative for $Fe_{22}Pt_{21}/CH_3CH_2COOH$, $Fe_{22}Pt_{21}/CH_3CH_2CH_2NH_2$, and $Fe_{22}Pt_{21}/CH_3CH_2CH_2SH$, respectively. For the ligands with longer hydrocarbon chains, only three adsorption configurations, **O**, **P**, and **Q** [Figs. 1(o)–1(q)], which have the same structures as the most stable configurations of the ligands with shorter chains (**E**, **G**, and **K**) were considered. For configurations **E** and **O**, two oxygen atoms bind to two different iron atoms via the COO bridging mode with the elimination of a hydrogen atom [Figs. 1(e) and 1(o)]. For configurations **G** and **P**, a nitrogen atom of NH_2 binds to an iron atom without the elimination of a hydrogen atom [Figs. 1(g) and 1(p)]. For configurations **K** and **Q**, a sulfur atom binds to an iron atom with the elimination of a hydrogen atom [Figs. 1(k) and (q)]. Starting from the initial structures, the geometrical structures were fully optimized without any constraints. For configurations involving the elimination of a hydrogen atom, the H atom was removed before the optimization.

IV. RESULTS AND DISCUSSION

A. The adsorption of ligands onto a FePt cluster

The bond lengths and adsorption energies calculated for the stable configurations (illustrated in Fig. 1) from the fully optimized configurations of the ligands adsorbed on the $Fe_{22}Pt_{21}$ clusters are summarized in Table I. The adsorption energy, E_b, is calculated as

$$E_{\mathrm{b}} = E_{\mathrm{Fe_{22}Pt_{21}}} + E_{\mathrm{ligand}} - E_{\mathrm{Fe_{22}Pt_{21}\text{ - ligand}}} \qquad (1)$$

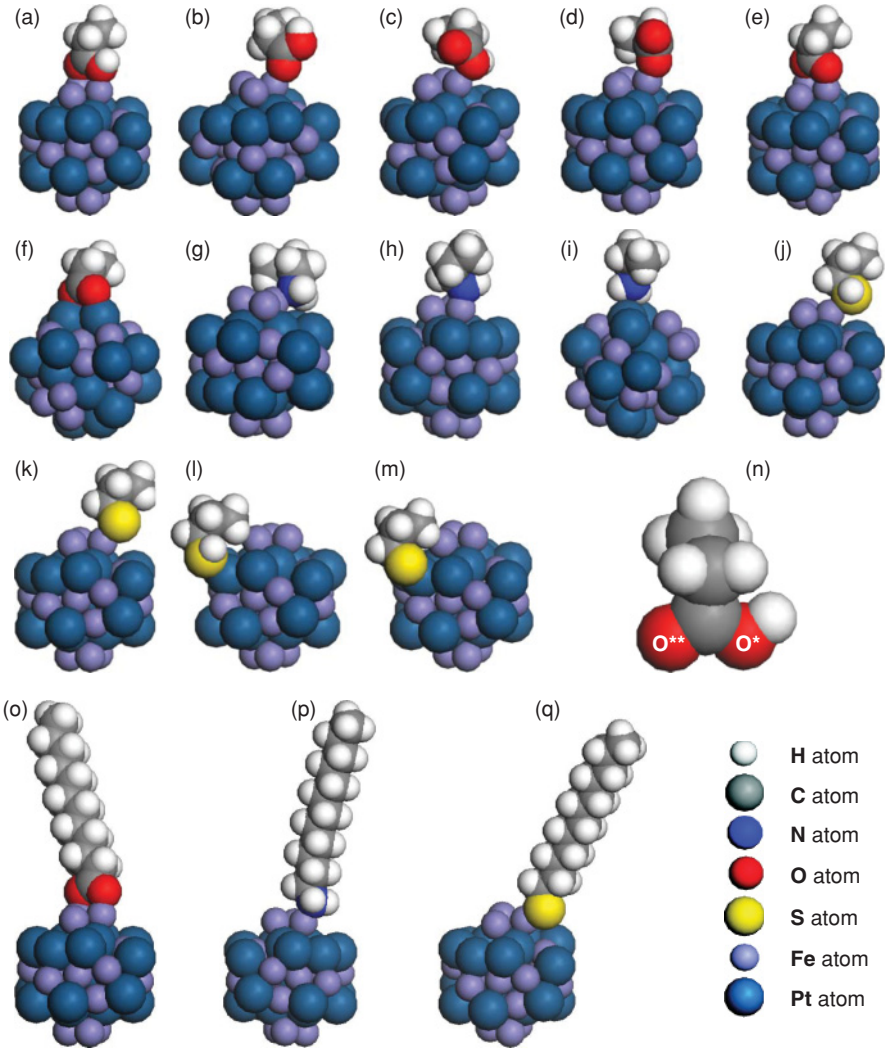

FIG. 1. (Color online) Some optimized configurations of $Fe_{22}Pt_{21}$ clusters containing different adsorbed ligands. (a–f) $Fe_{22}Pt_{21}/CH_3CH_2COOH$, (g–i) $Fe_{22}Pt_{21}/CH_3CH_2CH_2NH_2$, (j–m) $Fe_{22}Pt_{21}/CH_3CH_2CH_2SH$, (o) $Fe_{22}Pt_{21}/C_{11}H_{23}COOH$, (p) $Fe_{22}Pt_{21}/C_{11}H_{23}CH_2NH_2$, and (q) $Fe_{22}Pt_{21}/C_{11}H_{23}CH_2SH$, and (n) propionic acid.

for configurations **A**, **B**, **C**, **G**, **I**, **J**, **L**, and **P**, and

$$E_b = E_{Fe_{22}Pt_{21}} + E_{ligand} - \left(E_{Fe_{22}Pt_{21}\text{-ligand}} + 0.5E_{H_2}\right) \quad (2)$$

for configurations **D**, **E**, **F**, **H**, **K**, **M**, **O**, and **Q**, in which a hydrogen atom is eliminated from the functional group. Here, $E_{Fe_{22}Pt_{21}}$, E_{ligand}, $E_{Fe_{22}Pt_{21}\text{-ligand}}$, and E_{H_2} denote total energies of bare FePt cluster, free ligand, ligand-adsorbed FePt cluster, and hydrogen molecule, respectively. Unstable configurations are not shown. Configurations **A**-**F**, **G**-**I**, and **J**-**M** correspond to the adsorption of propanoic acid, propylamine, and propanethiol onto the cluster, respectively, where **A**-**E**, **G**, **H**, **J**, and **K** correspond to adsorption at Fe sites and the others to adsorption at Pt sites. The structures of these configurations are described in detail in Sec. III and are illustrated in Fig. 1. Because there are no experimental data for the bond lengths in similar systems, the experimental bond lengths from different molecular systems have been included in Table I for comparison. For FePt clusters containing adsorbed propanoic acid ($Fe_{22}Pt_{21}/CH_3CH_2COOH$), the Fe-O bond lengths are in good agreement with experimental data for Fe(II) complexes. The most stable configuration for the $Fe_{22}Pt_{21}/CH_3CH_2COOH$ system is **E** [$E_b = 3.49$ eV; Fig. 1(e)], which is bidentate with two oxygen atoms of the ligand chemically binding in a COO group bridging mode symmetrically to the surface of two iron atoms. The next most stable configuration is **D** [$E_b = 2.06$ eV; Fig. 1(d)], which is monodentate with one O* atom of the ligand chemically binding to the surface of the cluster at an Fe atom and the other O** atom remains uncoordinated.

These results are consistent with results from FT-IR spectroscopy for as-synthesized FePt NPs in the presence of a mixed oleic acid-and-oleylamine (1 : 1) surfactant,[8,9] where vibrations from both bidentate [-COO-M, M: metal, 1512 (Ref. 8) or 1551 (Ref. 9) cm^{-1}] and monodentate [-CO-M, 1709 (Ref. 8) or 1711 (Ref. 9) cm^{-1}] binding were observed. In addition, it was shown that the relative intensity of the bidentate peak was much higher than that of the monodentate peak.[8,9] After addition of dodecanethiol (DDT), only the bidentate peak remained due to a significant amount of oleic acid remaining undisplaced,[9] which suggests that bidentate binding of carboxylate groups to FePt NPs is more stable than monodentate coordination. Bagaria and coworkers[9] also confirmed the strong affinity of carboxylate groups for Fe atom from Fe_{2p} XPS spectra of the as-synthesized FePt NPs and those exchanged with DDT. On the other hand, it is difficult to obtain convergence of the structural optimization for most of the configurations where the ligand is adsorbed on the cluster at Pt atoms, because the structure of the ligand in these configurations tends to collapse to generate

TABLE I. Bond lengths and adsorption energies for the stable configurations of the $Fe_{22}Pt_{21}$ clusters containing adsorbed ligands. Fe^{i}, Fe^{iii}, and Fe^{iii} and Pt^{i}, Pt^{ii}, and Pt^{iii} represent different surface Fe and Pt atoms in the cluster that bind to O, N, or S atoms of the ligands; O^{*} and O^{**} represent the two O atoms of the carboxyl end group of CH_3CH_2COOH, where (*) and (**) indicate that the O atoms contain and lack an H atom, respectively; after adsorption O^{*} and $O^{*}(H)$ indicate that the H atom is eliminated and not eliminated, respectively. See Fig. 1 for further information.

Ligand	Configuration	Bond	Bond length d (Å) PBE GGA	Literature	Adsorption energy E_b (eV)
CH_3CH_2COOH	**A**	Fe^{ii}-$O^{*}(H)$	2.102		1.88
		Fe^{i}-O^{**}	1.910		
	B	Fe^{ii}-O^{**}	1.886		1.43
	C	Fe^{ii}-$O^{*}(H)$	2.135		1.10
	D	Fe^{ii}-O^{*}	1.823		2.06
	E	Fe^{ii}-O^{*}	1.966	1.75–1.90[a]	3.49
		Fe^{i}-O^{**}	1.964	1.872–1.951[b]	
	F	Pt^{iii}-O^{*}	2.192	2.058, 2.069[c]	0.91
		Pt^{ii}-O^{**}	2.257	2.34[d]	
$CH_3(CH_2)_2NH_2$	**G**	Fe^{iii}-$N(H_2)$	2.114	1.95–2.30[a]	1.71
	H	Fe^{iii}-N(H)	1.856		1.04
	I	Pt^{i}-$N(H_2)$	3.163	2.17[d]	0.15
$CH_3(CH_2)_2SH$	**J**	Fe^{ii}-S(H)	2.480		1.13
	K	Fe^{ii}-S	2.245	2.28[e]	1.71
	L	Pt^{i}-S(H)	2.471		0.64
	M	Pt^{i}-S	2.322	2.334, 2.335[d]	0.84
$C_{11}H_{23}COOH$	**O**	Fe^{ii}-O^{*}	1.950		3.33
		Fe^{i}-O^{**}	1.961		
$C_{11}H_{23}CH_2NH_2$	**P**	Fe^{iii}-$N(H_2)$	2.128		1.51
$C_{11}H_{23}CH_2SH$	**Q**	Fe^{ii}-S	2.242		1.48

[a]The Fe K edge extended x-ray absorption fine structure (EXAFS) analysis for alternative Fe-O_2 bond lengths in Fe(II) porphyrin-O_2 adducts, Ref. 31.

[b]Single crystal x-ray data for an iron(III) oxide cluster containing two different discrete $[Fe_3O]$ units: $[Fe_3O(O_2CCHCHCH_3)_6(H_2O)_3]$ and $[Fe_3O(O_2CCHCHCH_3)_7(H_2O)_2](HO_2CCHCHCH_3)_4(OH)(H_2O)$, Ref. 32.

[c]Single crystal x-ray data for Pt(II) complexes, Ref. 33.

[d]EXAFS for octahedral Pt(IV) complexes in a hexameric trimethylplatinum theophylline system (Pt-N: 2.17 Å, Pt-O: 2.34 Å) and Pt(II) complexes in a guanine complex (Pt-N: 2.02–2.06 Å), Ref. 34.

[e]XAFS for a protein, Ref. 35.

hydrogen atoms or other small hydrocarbon species, resulting in negative adsorption energies (data not shown). Although the convergence difficulties might be also caused by an existence of reaction barriers, we have not considered the transition state in the present study. Configuration **F** ($E_b = 0.91$ eV, Fig. 1(f)) was found to be the most stable orientation for the adsorption of ligands at Pt atoms.

A similarity is found in the adsorption of propylamine on the surface of the FePt cluster ($Fe_{22}Pt_{21}/CH_3CH_2CH_2NH_2$). Configuration **G** [$E_b = 1.71$ eV; Fig. 1(g)], in which propylamine is adsorbed on the cluster at an Fe site with the NH_2 group intact, is the most stable. The next most stable configuration is **H** [$E_b = 1.04$ eV; Fig. 1(h)], in which an N atom binds to Fe and a hydrogen atom is eliminated before the geometry optimization. These results support the FT-IR spectra obtained for the as-synthesized FePt NPs in the presence of a mixture of oleic acid and oleylamine (1:1).[8,9] For instance, the coexistence of both of these configurations are confirmed by Shukla *et al.*,[8] where vibration modes of both NH_2-M (1593 cm^{-1}) and NH-M (3300 cm^{-1}) were found. The intensity of the NH_2-M peak was much higher than that of the NH-M peak. Bagaria *et al.*[9] did not observe the NH-M vibration mode for their FePt NPs; only the NH_2-M (1591 cm^{-1}) mode, which suggests that binding of an intact NH_2 group to FePt NPs is the dominant configuration. However, it has not yet been proven experimentally whether oleylamine is adsorbed on FePt NPs at Fe or Pt atoms. Our results reveal that the adsorption of propylamine at a Pt site is quite unstable from an energetic point of view; for example, configuration **I** [Fig. 1(i)], in which propylamine is adsorbed on the cluster with the NH_2 group intact, also has a very small adsorption energy ($E_b = 0.15$ eV) and the configuration in which a nitrogen atom binds to Pt with the generation of a hydrogen atom exhibits a negative adsorption energy (data not shown). In addition, the Fe-$N(H_2/H)$ bond lengths of configurations **G** and **H** are consistent with experimental data, while the Pt-$N(H_2)$ bond length of configuration **I** is much larger than typical experimental values for chemical bonds of Pt(II/IV) complexes.

In the case of the adsorption of propanethiol on the FePt cluster ($Fe_{22}Pt_{21}/CH_3CH_2CH_2SH$), the calculated adsorption energies for all four configurations **J**, **K**, **L**, and **M** [Figs. 1(j)–(m)], which are 1.13, 1.71, 0.64, and 0.84 eV, respectively, are fairly similar. This distinct feature for the case of

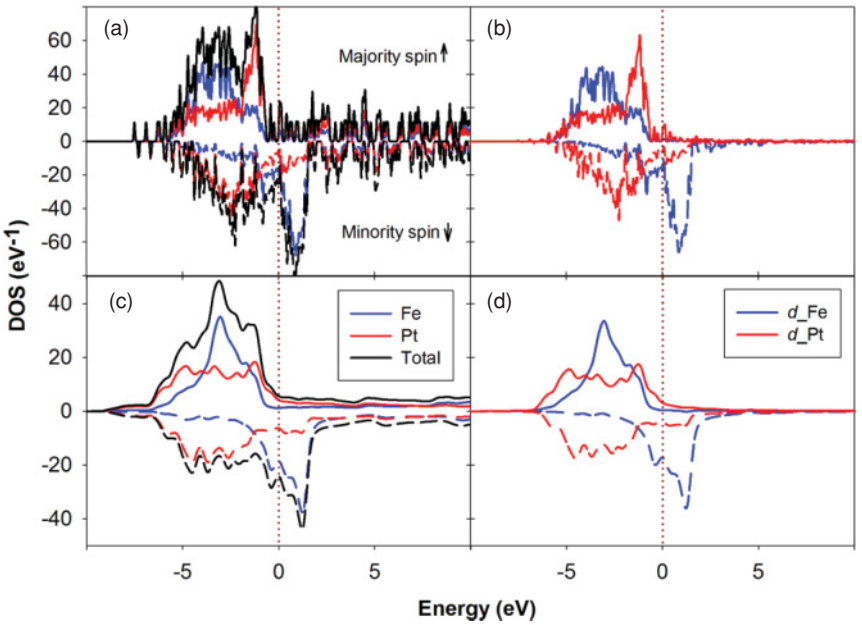

FIG. 2. (Color online) DOS and PDOS of Fe and Pt atoms in (a) a bare *fcc*-$Fe_{22}Pt_{21}$ cluster and (c) bulk *fcc*-FePt and *d*-state PDOS of Fe and Pt atoms in (b) a bare *fcc*-$Fe_{22}Pt_{21}$ cluster and (d) bulk *fcc*-FePt. Dotted lines indicate Fermi levels.

propanethiol suggests that some configurations may coexist, that is, propanethiol is adsorbed on the surface of the cluster at both Fe and Pt sites. The adsorption of thiol on FePt NPs at Pt sites was confirmed experimentally from S_{2p} and Pt_{4f} XPS spectra of the as-synthesized FePt NPs exchanged with DDT.[9]

In terms of energy, the most stable structures for the ligands adsorbed on the cluster are configurations **E** (3.49 eV), **G** (1.71 eV), and **K** (1.71 eV) for the $Fe_{22}Pt_{21}/CH_3CH_2COOH$, $Fe_{22}Pt_{21}/CH_3CH_2CH_2NH_2$, and $Fe_{22}Pt_{21}/CH_3CH_2CH_2SH$ systems, respectively. All of the ligands investigated prefer to adsorb on the surface of the FePt cluster at Fe sites rather than Pt sites, and bidentate configuration **E** is the most stable of all. This result is consistent with the experimental observation of the strong affinity of Fe for carboxylate groups, even after DDT was added to FePt NPs containing adsorbed oleic acid a significant amount of oleic acid remained bound to Fe in a bidentate fashion.[9] Our calculations may provide insight into the adsorption of ligands onto FePt NPs in the actual synthesis of FePt NPs, where an excess of ligands (e.g., oleic acid and oleylamine) is often used to stabilize the FePt NPs. Adsorption may take place with competition between energetic priority and the steric effects of the adsorbed ligands. In detail, the ligands possessing a carboxyl end group are first adsorbed on FePt NPs at Fe sites in bidentate and monodentate configurations. Adsorption then mainly occurs on Pt sites and the steric effects may dominate, so ligands with amine or thiol groups have the opportunity to become adsorbed on the FePt NPs at Pt sites because they have less steric demand compared to the carboxyl group. In fact, the FePt NPs synthesized in the presence of a mixture of oleic acid and oleylamine (1:1) contain oleic acid bound to Fe atoms in both bidentate and monodentate fashions, and, after addition of DDT, thiol groups displace amine moieties to bind to Pt atoms. Our results are in agreement with experimental work,[9] which shows that it is necessary to employ a combination of different ligands, such as carboxyl and thiol ligands, to stabilize FePt NPs through bonding at both Fe and Pt sites.

B. Ligand-FePt interactions

To understand the interactions between the FePt cluster and different ligands, the electronic structures of the bare FePt cluster and the organic ligands, as well as the clusters containing adsorbed ligands, were investigated. The total density of states (DOS) of the chemically disordered *fcc*-$Fe_{22}Pt_{21}$ cluster and the projected density of states (PDOS), and the *d*-state PDOS of Fe and Pt atoms are shown in Figs. 2(a) and 2(b). Obviously, the main features of the Fe partial PDOS and *d*-state PDOS are relatively narrow because of the localized orbitals and strong exchange splitting. The exchange splitting results in local magnetic moments. For Pt, the minority PDOS is increased slightly above the Fermi level due to the hybridization of the Pt 5*d* states with Fe 3*d* states, as seen for a small unoccupied state just above the Fermi level in the PDOS. These features are strikingly similar to those for the chemically disordered bulk *fcc*-FePt, as seen in Figs. 2(c) and 2(d). Despite these similarities, a closer inspection reveals that the DOS and PDOS of the cluster are discretized because of the electron confinement in a low-dimensional nanostructure (0D). As shown in Fig. 2(a), the large exchange splitting between the majority spin and minority spin in the PDOS of the Fe atom compared to that of the Pt atom results in the Fe atom making the primary contribution to the spin magnetic moment in FePt. In addition, Fig. 2(b) reveals that the number of Fe *d* states in the minority spin around the Fermi level, especially the unoccupied states just above the Fermi level, is significantly larger than that of the Pt *d* states in the minority spin, which causes a large difference in their interaction with the ligands.

To understand the features of the interaction between a ligand and a cluster, we analyzed the *d*-state PDOS of specific Fe (Fe^{i}, Fe^{ii}, and Fe^{iii}) atoms and *p*-state PDOS of O (O^{*} and O^{**}), N, and S atoms at the adsorption sites before and after adsorption at Fe sites, as shown in Figs. 3(a)–3(g). In addition, to explore the reason for the preferred adsorption at Fe sites, an analysis of the *d*-state PDOS of specific Pt (Pt^{i}, Pt^{ii}, and Pt^{iii}) atoms and the *p*-state PDOS of the atoms adsorbed at Pt sites was also performed [Figs. 3(h)–3(n)]. For comparison,

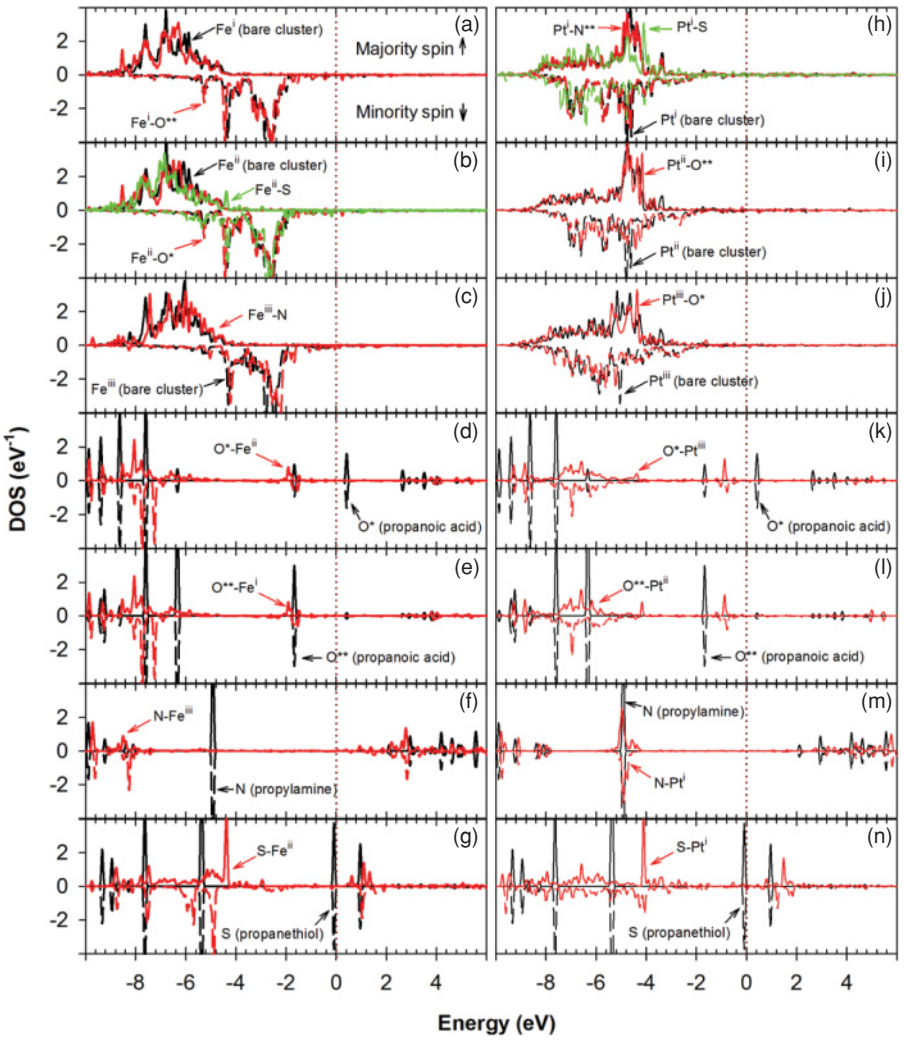

FIG. 3. (Color online) *d*-state PDOS of specific Fe atoms including (a) Fe^{i}, (b) Fe^{ii}, and (c) Fe^{iii}, Pt atoms including (h) Pt^{i}, (i) Pt^{ii}, and (j) Pt^{iii}, and *p*-state PDOS of O atoms including O* (d) and (k), and O** (e) and (l), an N atom (f) and (m), and an S atom (g) and (n) for the bare ligands (propanoic acid $E_F = -3.19$ eV, propylamine $E_F = 0.00$ eV, and propanethiol $E_F = -3.19$ eV), bare $fcc - Fe_{22}Pt_{21}$ cluster ($E_F = -3.49$ eV), **E** ($E_F = -3.65$ eV), **G** ($E_F = -3.38$ eV), **K** ($E_F = -3.71$ eV), **F** ($E_F = -3.67$ eV), **I** ($E_F = -3.49$ eV), and **M** ($E_F = -3.57$ eV). The black and colored curves correspond to before and after adsorption at Fe [(a)–(g)] and Pt [(h)–(n)] sites, respectively. For clarity, Fermi levels are not indicated in this figure.

all of the PDOS curves were normalized and plotted in terms of absolute energy without shifting the Fermi level E_F.

For adsorption at an Fe site, the position of the original PDOS peaks of the Fe atoms [Figs. 3(a)–3(c)] in the bare cluster ($E_F = -3.49$ eV) compared to those of the O, N, and S atoms [Figs. 3(d)–3(g)] in the bare ligands, including propanoic acid ($E_F = -3.19$ eV), propylamine ($E_F = 0.00$ eV), and propanethiol ($E_F = -3.19$ eV), suggests that there is a possibility for hybridization between the occupied majority *d*-states of the Fe atoms and the occupied majority *p* states of O, N, and S atoms, and between the unoccupied minority *d*-state of Fe atoms and unoccupied minority *p* states of O and S atoms. Indeed, the *d* and *p* states PDOS of the specific atoms after adsorption become boarder and the majority spin is much broader than that of the minority [Figs. 3(a)–3(g), implying strong hybridization between the occupied majority *p* and *d* states of these atoms. These hybridizations suggest that the interaction has a strong covalent nature; this was also confirmed by the difference in charge density, which will be discussed in the following part.

However, the significant change in the *p* states of O, N, and S atoms after adsorption [Figs. 3(d)–3(g)] is difficult to interpret. Therefore, we also created an interaction model for configurations **E**, **G**, and **K** to determine the changes in their density of states on adsorption. For the model, the ligands are adsorbed on the cluster at a distance (D) from surface of the cluster to the polar end groups of the ligands, and the interaction versus D between the ligand and the cluster was investigated in a fixed direction from the cluster. The distance $D = 0.0$ Å corresponds to the optimized cluster with adsorbed ligands that has the strongest interaction between the ligands and FePt cluster. The bare ligands have no interaction with the cluster and the interaction increases as D decreases. The interaction of the acid and thiol ligands with the cluster is similar; far from the cluster ($D = 2$ Å), the *p*-state PDOS form new unoccupied states at ca. 0.6 eV for O [Figs. 4(a) and 4(b)] and ca. 1.8 eV for S [Fig. 4(d)], and new occupied states around Fermi levels at ca. −4.0 eV for O [Figs. 4(a) and 4(b)] and ca. −3.8 eV for S [Fig. 4(d)]. These new states originate from the elimination of hydrogen atoms before geometry optimization and gradually shift to lower energy as the distance decreases ($D = 0.5$ and 0.0 Å). This is a result of the competition between the strong hybridization of the occupied majority *p* states of O or S atoms and the *d* states of Fe atoms and the electron transfer from Fe atoms to O or S atoms. The hybridization decreases the energy of the *p* states, while the electron transfer has the opposite effect. The adsorption of propylamine onto the cluster with NH_2 intact (without the elimination of hydrogen)

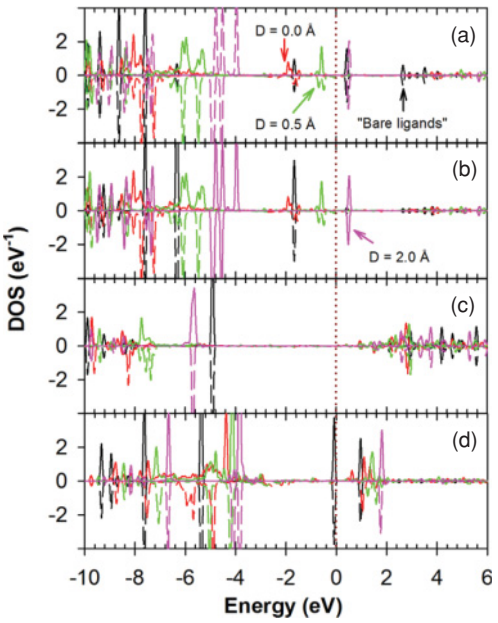

FIG. 4. (Color online) p-state PDOS of (a) O*, (b) O**, (c) N, and (d) S atoms corresponding to the interaction distance, D, from the surface of the cluster and the polar end group of the ligands for the bare ligands, $Fe_{22}Pt_{21}/C_2H_5COO$, $Fe_{22}Pt_{21}/C_3H_7NH_2$, and $Fe_{22}Pt_{21}/C_3H_7S$. "Bare ligands" (black curves) represents propanoic acid, propylamine, and propanethiol without interaction with the cluster, $D = 0.0$ Å (red curves) for the optimized clusters with adsorbed ligands, including configurations **E**, **G**, and **K**, and $D =$ 0.5 (green curves) and 2.0 Å (pink curves) for the systems in which the distance between the ligand and cluster is increased in a fixed direction. For clarity, Fermi levels are not indicated in this figure.

via a lone pair electrons on N present different interactions. The combination of hybridization and electron transfer from N to Fe atoms pushes the p states of the N atom to lower energy, as seen in Fig. 4(c).

The electron transfer characteristics were confirmed by Mulliken population analysis, which showed that a very small amount of electron density equivalent to 0.133 e and 0.005 e is transferred from Fe atoms to O and S atoms in configurations **E** and **K**, respectively, and involves d-, p-, and s-state electrons. These results seem feasible given the electron-accepting nature of carboxylate and thiolate groups due to the larger Mulliken

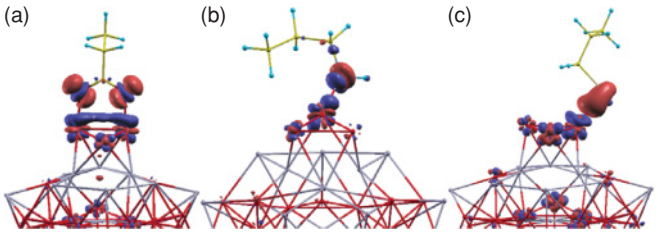

FIG. 5. (Color online) Isosurfaces of the difference in charge density $[\Delta\rho = \rho_{\text{FePt-ligand}} - (\rho_{\text{FePt}} + \rho_{\text{ligand}})]$ on the adsorption of single organic ligands onto FePt clusters for configurations (a) **E**, (b) **G**, and (c) **K**. The isovalue of the spin electron density used was 6×10^{-3}. Blue and red colors indicate a decrease and increase in the total charge density, respectively.

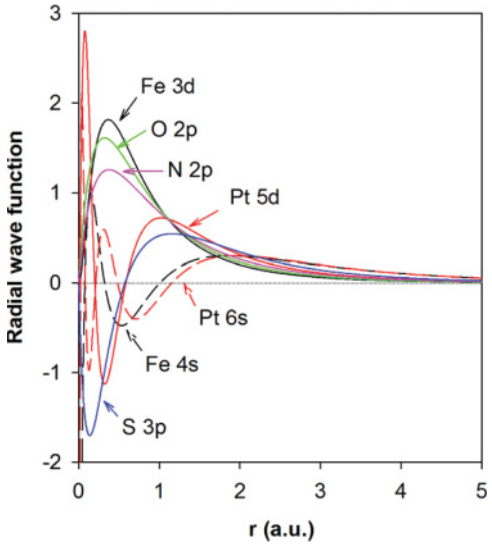

FIG. 6. (Color online) Radial wave functions of Fe, Pt, O, N, and S atoms generated using an ADPACK code.[25]

electronegativities of O and S compared to that of Fe. Mulliken electronegativities calculated using a linear transformation [$\chi_M = 0.18 \times (E_i + E_{ea}) + 0.17$; E_i: ionization energy, E_{ea}: electron affinity][36] for the first ionizations of O, S, and Fe atoms were 2.99, 2.49, and 1.68 eV, respectively. In contrast, for configuration **G**, the equivalent of 0.029 e is transferred from the N atom to the Fe atom. This result may be understood by considering the electron-donating nature of amino groups caused by the lone pair of electrons on the N atom. This finding is also consistent with a recent spin-polarized DFT calculation by Wu *et al.* of cluster models of FePt(111), including a molecule of oleylamine.[6] Their results showed that charge was transferred to the surface Fe site from oleylamine. The small amount of electron transfer is reflected in the minority d-state PDOS of the Fe atom, which shows a very slight shift to lower energy in configuration **E** [Fig. 3(a) and 3(b)], is nearly unchanged for configuration **K** [Fig. 3(b)], and moves to higher energy for configuration **G** [Fig. 3(c)]. These results suggest the interactions between these ligands and Fe atoms have a weak ionic nature.

In addition, the charge reorganization around Fe, and the O, N, and S atoms of the ligands after adsorption was characterized by differences in the charge density induced by the interaction, as shown in Fig. 5. The total charge of clusters containing adsorbed ligands was calculated first, and the charges of the separate ligands and cluster were then calculated by maintaining the same atomic positions. Finally, the difference in charge density was estimated by extracting the charge of the ligands and cluster from that of the clusters containing adsorbed ligands. The results reveal that electrons accumulated along Fe-O (N or S) bonds, which originate from Fe and O, N, or S atoms and suggests the formation of covalent Fe-O (N or S) bonds. In particular, electron density accumulated near O and S atoms rather than near Fe atoms in configurations **E** [Fig. 5(a)] and **K** [Fig. 5(c)]; while electron density is localized at N atoms in configuration **G** [Fig. 5(b)]. These results reflect the high electronegativity of O and S atoms compared to Fe and the presence of the lone pair of

TABLE II. Average spin magnetic moments (μ_B, Bohr magneton) of Fe atoms in various structures and phases in comparison with available experimental data and other calculation results.

Structure		Disordered *fcc*-FePt	Ordered *fcc*-FePt	Ordered *fct* ($L1_0$)-FePt
Bulk crystal	PBE GGA	3.06	3.13	3.16
	Literature	2.92 ± 0.29[a], 3[b]	NA	2.80[e], 2.96[f]
Surface	(0 0 1)	NA	3.17	3.20
	(1 0 0)	NA	3.24	3.26
	(1 1 0)	NA	3.22	3.23
	(1 1 1)	NA	3.20	3.21
Bare cluster	PBE GGA	3.21	3.32	3.32
	Literature	3.40 ± 0.3[c], 2.48 ± 0.25[d]	NA	2.59 ± 0.26[g]
Clusters with adsorbed ligands	**E**	3.21	NA	NA
	G	3.21	NA	NA
	K	3.22	NA	NA
	O	3.21	NA	NA
	P	3.21	NA	NA
	Q	3.22	NA	NA

[a]Using x-ray magnetic circular dichroism (XMCD) at the $L_{2,3}$ edges of Fe, Ref. 39.
[b]DFT calculation, Ref. 40.
[c]Using XMCD at the $L_{2,3}$ edges of Fe (for bare 6.5 nm *fcc*-FePt NPs prepared in H_2 plasma), Ref. 41.
[d]Using XMCD at the $L_{2,3}$ edges of Fe (for bare 6.3 nm *fcc*-FePt NPs prepared by soft H_2 plasma), Ref. 42.
[e]Experimental data, Ref. 43.
[f]Using the full-potential linear muffin-tin orbital method within GGA, Ref. 44.
[g]Using XMCD at the $L_{2,3}$ edges of Fe (for bare *fct*-FePt NPs prepared by annealing of 6.3 nm *fcc*-FePt NPs), Ref. 42.

electrons on the N atom. Overall, our results show that the interaction of the ligands with the cluster has a strong covalent and weak ionic nature.

Interestingly, comparison of the *p*-state PDOS peaks of O, N, and S after adsorption with before adsorption at both Fe [Figs. 3(d)–3(g)] and Pt sites [Figs. 3(k)–3(n)] reveals that for adsorption at Fe sites, the *p*-state PDOS increase in energy more than for those from adsorption at Pt sites. For example, for the adsorption of propylamine onto the cluster, the position of the N *p*-state PDOS of the bare propylamine at ca. −4.90 eV is shifted significantly to ca. −8.40 eV after adsorption at a Fe site (Fig. 3(f)) and remains unchanged after adsorption at a Pt site [Fig. 3(m)]. Furthermore, the radial wave functions of a Pt (5*d* and 6*s*) atom are more delocalized than those of a Fe (3*d* and 4*s*) atom, as seen in Fig. 6. This may mean that the distances of Pt-O (N or S) bonds are longer than those of Fe-O (N or S) bonds. These results suggest that adsorption is preferred at Fe sites over Pt sites. Additionally, the radial wave function of S (3*p*) is significantly more delocalized than that of O (2*p*) and N (2*p*) so the difference between the Fe-S and Pt-S bond lengths is the smallest compared to the other two values. Indeed, the bond length differences calculated from Table I are 0.077 (Pt^{i}-S − Fe^{ii}-S), 0.293 (Pt^{ii}-O** − Fe^{i}-O**), and 0.126 (Pt^{iii}-O* − Fe^{ii}-O*) and 1.049 [Pt^{i}-N(H_2) − Fe^{iii}-N(H_2)] Å for the pairs of configurations **K** and **M**, **E** and **F**, and **G** and **I** for $Fe_{22}Pt_{21}/C_3H_7S$, $Fe_{22}Pt_{21}/C_2H_5COO$, and $Fe_{22}Pt_{21}/C_3H_7NH_2$ systems, respectively. This also suggests that S atoms can bind to Pt atoms in the adsorption of thiol ligands on the cluster as a result of the adsorption energy mentioned above.

C. Magnetic properties

Magnetic ground states were identified by performing spin-polarized calculations with ferromagnetic alignment of atomic spins. As a consequence of the large separation between the majority and minority spins in the PDOS of Fe atoms, Fe atoms provide the primary contribution to the spin magnetic moment in FePt. Also, adsorption takes place preferentially at Fe sites rather than at Pt sites; therefore, we consider here only the spin magnetic moment of the Fe atom to examine the influence of the interaction of FePt with a ligand on its magnetic properties. The calculated average spin magnetic moments of Fe for the bare *fcc*-$Fe_{22}Pt_{21}$ cluster and the clusters containing adsorbed ligand, including configurations **E**, **G**, and **K** for the ligands with shorter hydrocarbon chains and **O**, **P**, and **Q** for the ligands with longer chains, as well as that for bulk *fcc*-FePt, are summarized in Table II. For the following comparison and discussion, the magnetic moments of Fe in ordered *fcc*-FePt and *fct* ($L1_0$)-FePt in various phases, including bulk and surface and as bare clusters, were also calculated. The calculated spin magnetic moments are found to be well agreed with experimental data available in the literatures.[39,41–43]

For the bare disordered *fcc*-$Fe_{22}Pt_{21}$ cluster, the average magnetic moment of the Fe atom is considerably larger compared with that of disordered bulk *fcc*-FePt and is even higher than that of bulk $L1_0$-FePt. Our result is fully in accordance with experimental data of Boyen *et al.*[37] and calculation results by Ebert *et al.*[38] This enhanced moment may well result from the large surface of the FePt cluster caused by the finite size effect in low-dimensional systems. The average spin magnetic moments of the Fe atoms are unchanged in the clusters containing adsorbed ligands compared to those of the bare cluster, even for the clusters capped with ligands possessing longer hydrocarbon chains. However, the spin magnetic moment of the Fe atoms at adsorption sites decreased

TABLE III. Spin magnetic moment (μ_B) of Fe atoms at adsorption sites in configurations **E**, **G**, **K**, **O**, **P**, and **Q**.

Adsorption site	Before adsorption	After adsorption					
		E	**G**	**K**	**O**	**P**	**Q**
Fe^{i}	3.26	3.24			3.24		
Fe^{ii}	3.26	3.23		3.20	3.21		3.22
Fe^{iii}	3.22		3.15			3.15	

slightly and a rather small range of data was found for the various systems investigated, as shown in Table III.

These small reductions in the spin magnetic moments result from the strong hybridization between the majority *p* states of oxygen, nitrogen, or sulfur of the ligands and the majority *d* states of Fe in the cluster on their interaction, which decreases the majority spin of the *d* states of Fe [Fig. 3(a)–3(c)] and thus decreases the spin magnetic moments. The charge transfer is very small, around 0.133 *e* and 0.005 *e* from Fe atoms to oxygen and sulfur atoms for configurations **E** and **K**, respectively, and 0.029 *e* from a nitrogen atom to an Fe atom for configuration **G**; therefore, the contribution of charge transfer to the magnetic moments can be neglected. This small difference in the spin magnetic moment of Fe was also reflected by a slight difference in the decomposed *d*-state PDOS of Fe before and after adsorption (data not shown). Another possibility for the reduction in the spin magnetic moment is that the Fe atom at the surface became more symmetrical after adsorption because more of its coordination sites are occupied with ligands. The increased symmetry causes the Fe atoms to possess similar magnetic features to Fe atoms inside the cluster; therefore, the spin magnetic moment decreased.

In addition, the spin magnetic moments of Fe at the adsorption sites for the cluster capped with the ligands with longer hydrocarbon chains (configurations **O**, **P**, and **Q**) do not change compared to those of the ligands with shorter chains (configurations **E**, **G**, and **K**), as seen in Table III. This result is unlike the previous experimental observation of a dramatic decrease in the saturation magnetization of FePt capped with ligands with longer versus shorter chains.[7] The discrepancy between theoretical and experimental results may arise from the limitation of our study. In the present theoretical study, we focused only on the influence of ligands on the spin magnetic moment of Fe by analyzing its electronic structure. Spin magnetic anisotropy, spin configuration, and conformational change should be considered to obtain more accurate results in terms of the reduction of saturation magnetization of FePt NPs. These influences will be further investigated in the future. The slight reduction of the magnetic moment of Fe for configurations **O**, **P**, and **Q** compared with those for bulk *fcc*-FePt and a bare *fcc*-FePt cluster has the same mechanism as described for configurations **E**, **G**, and **K**. That is, the interplay between the strong hybridization and minimal electron transfer and the reduction of the surface magnetic moment after adsorption because of the symmetrical coordination of the surface Fe atoms by the ligands.

The spin magnetic moments of Fe at adsorption sites have been found to be slightly decreased after the adsorption of organic ligands. However, one can rationalize the significant reduction of the saturation magnetization of FePt NPs observed previously[6,7] by expanding the mechanism of the influences of the ligands on the cluster described above to FePt NPs synthesized by wet chemistry, where NPs have a large specific surface area and are densely packed by organic ligands. Because the surface dependence of magnetism does play a significant role in the enhancement of the spin magnetic moment of FePt clusters, while the adsorption of ligands takes place on the surface resulting in a reduction of the spin magnetic moment. As the results of electronic structure calculations for all surfaces investigated (001), (100), (110), and (111) in both ordered *fcc*- and $L1_0$-FePt, the spin magnetic moments of the Fe atoms are higher than those of bulk and cluster (Table II) and increased from the inner shells to the outer shells. The magnetic moments of Fe atoms in the outermost shell are significantly enhanced, and inner Fe atoms have magnetic moments approaching the value found for bulk FePt (data not shown).

V. CONCLUSION

First-principle calculations were performed to investigate the structural, electronic, and magnetic properties of binary FePt systems. Our results show that the interaction between FePt clusters and various ligands has a strong covalent and weak ionic nature, and the ligands prefer to adsorb at Fe sites rather than Pt sites on the surface of the FePt cluster. For the FePt clusters containing an adsorbed carboxylate ligand, a bidentate configuration in which two oxygen atoms bind almost symmetrically to two different Fe atoms on the surface is the most stable structure. For the FePt clusters containing an adsorbed thiolate ligand, configurations may coexist, meaning the ligand can be adsorbed at either Fe or Pt sites. The spin magnetic moment of Fe atoms at adsorption sites decreases slightly because of the strong hybridization of the majority *d* states of Fe atoms with majority *p* states of O, N, and S atoms and the electron transfer between the ligands and Fe atoms on the surface of the clusters involving *d*, *p*, and *s* states of Fe atoms. The reduction of the magnetic moment of Fe also originates from the increased symmetry of surface Fe atoms on coordination of a ligand. Adsorption of ligands with longer hydrocarbon chain does not change the magnitude of the spin magnetic moment of the Fe atoms compared to the complexes containing ligands with shorter chains.

In our investigation, all of the configurations investigated have only a single ligand molecule adsorbed onto the cluster; therefore, the magnetic moment does not change significantly on the adsorption of the ligand. In addition, the global minimum energy for the initial FePt cluster was not determined so our initial cluster might have not possessed the global minimum energy. The influence of surface ligands on the magnetic properties is not fully understood by means of the spin magnetic moment of Fe on interaction with various ligands. Several other parameters such as spin magnetic anisotropy, spin configuration, and change of geometrical structures should be considered and warrant further investigation.

ACKNOWLEDGMENTS

The authors thank to Dr. Dam Hieu Chi, JAIST, for his kind help in the use of MATERIALS STUDIO. This work was supported by the Ministry of Education, Culture, Sports, Science and Technology of Japan within the Graduate School Educational Reform Support Program.

---

*t-ozaki@jaist.ac.jp
†shinya@jaist.ac.jp

[1]S. Maenosono and S. Saita, IEEE Trans. Magn. **42**, 1638 (2006).
[2]J. S. Choi, Y. W. Jun, S. I. Yeon, H. C. Kim, J. S. Shin, and J. Cheon, J. Am. Chem. Soc. **128**, 15982 (2006).
[3]S. Sun, Adv. Mater. **18**, 393 (2006).
[4]C. J. Xu and S. H. Sun, Polym. Int. **56**, 821 (2007).
[5]S. Laurent, D. Forge, M. Port, A. Roch, C. Robic, L. V. Elst, and R. N. Muller, Chem. Rev. **108**, 2064 (2008).
[6]X. W. Wu, C. Liu, L. Li, P. Jones, R. W. Chantrell, and D. Weller, J. App. Phys. **95**, 6810 (2004).
[7]Y. Tanaka, S. Saita, and S. Maenosono, Appl. Phys. Lett. **92**, 093117 (2008).
[8]N. Shukla, C. Liu, P. M. Jones, and D. Weller, J. Magn. Magn. Mater. **266**, 178 (2003).
[9]H. G. Bagaria, E. T. Ada, M. Shamsuzzoha, D. E. Nikles, and D. T. Johnson, Langmuir **22**, 7732 (2006).
[10]M. Weinert and J.W. Davenport, Phys. Rev. Lett. **54**, 1547 (1985).
[11]C. S. Feigerle, A. Seiler, J. L. Pena, R. J. Celotta, and D. T. Pierce, Phys. Rev. Lett. **56**, 2207 (1986).
[12]K. C. Hass, M.-H. Tsai, and R. V. Kasowski, Phys. Rev. B **53**, 44 (1996).
[13]S. R. Chubb and W. E. Pickett, Phys. Rev. B **38**, 10227 (1988).
[14]B. Sinkovic, P. D. Johnson, N. B. Brookes, A. Clarke, and N. V. Smith, Phys. Rev. B **52**, R6955 (1995).
[15]F. Delbecq and P. Sautet, Chem. Phys. Lett. **302**, 91 (1999).
[16]H. Huang and J. Hermanson, Phys. Rev. B **32**, 6312 (1985).
[17]S. R. Chubb and W. E. Pickett, Phys. Rev. Lett. **58**, 1248 (1987).
[18]R. Wu and A. J. Freeman, Phys. Rev. B **45**, 7532 (1992).
[19]P. Hohenberg and W. Kohn, Phys. Rev. **136**, B864 (1964); W. Kohn and L. J. Sham, *ibid*. **140**, A1133 (1965).
[20]J. P. Perdew, K. Burke, and M. Ernzerhof, Phys. Rev. Lett. **77**, 3865 (1996).
[21]N. Troullier and J. L. Martins, Phys. Rev. B **43**, 1993 (1991).
[22]T. Ozaki, Phys. Rev. B **67**, 155108 (2003); T. Ozaki and H. Kino, *ibid*. **69**, 195113 (2004).
[23]J. M. Soler, E. Artacho, J. D. Gale, A. Garcia, J. Junquera, P. Ordejon, and D. Sanchez-Portal, J. Phys.: Condens. Matter **14**, 2745 (2002).
[24]T. Ozaki and H. Kino, Phys. Rev. B **72**, 045121 (2005).
[25][http://www.openmx-square.org/].
[26]V. L. Sedov, *Antiferromagnetism of γ-Fe: The Invar Problem* (Nauka, Moscow, 1987) [in Russian].
[27]R. Hayn and V. Drchal, Phys. Rev. B **58**, 4341 (1998).
[28]Joint Committee on Powder Diffraction Standards (JCPDS), card no. 43-1359.
[29]M. Müller, P. Erhart, and K. Albe, Phys. Rev. B **76**, 155412 (2007).
[30][http://accelrys.com/products/materials-studio/].
[31]G. L. Woolery, M. A. Waiters, K. S. Suslick, L. S. Powers, and T. G. Spiro, J. Am. Chem. Soc. **107**, 2370 (1985).
[32]K.-L. Zhang,Y.-J. Shi, S. Gao, Y.-D. Dai, K.-B. Yu, and X.-Z. You, Inorg. Chem. Commun. **7**, 584 (2004).
[33]A. Pasini, S. Rizzato, and D. De Cillis, Inorg. Chim. Acta **315**, 196 (2001).
[34]B. Lippert, *Cisplatin: Chemistry and Biochemistry of a Leading Anticancer Drug* (Wiley, New York, 1999), p. 326.
[35]R. Cammack and A. G. Sykes, *Advances in Inorganic Chemistry: Iron-Sulphur Proteins* (Academic Press, New York, 1992), p. 53.
[36]J. E. Huheey, *Inorganic Chemistry,* 2nd ed. (Harper & Row, New York, 1978), p. 167.
[37]H. G. Boyen *et al*., in *Verhandlungen der Deutschen Physikalischen Gesellschaft* (German Physical Society, Hamburg, 2004), p. 253.
[38]H. Ebert, S. Bornemann, J. Minár, P. H. Dederichs, R. Zeller, and I. Cabria, Comput. Mater. Sci. **35**, 279 (2006).
[39]C. Antoniak, M. Spasova, A. Trunova, K. Fauth, M. Farle, and H. Wende, J. Phys.: Conf. Ser. **190**, 012118 (2009).
[40]S. Ostanin, S. S. A. Razee, J. B. Staunton, B. Ginatempo, and E. Bruno, J. Appl. Phys. **93**, 453 (2003).
[41]H.-G. Boyen, K. Fauth, B. Stahl, P. Ziemann, G. Kästle, F. Weigl, F. Banhart, M. Hessler, G. Schütz, N. S. Gajbhiye, J. Ellrich, H. Hahn, M. Büttner, M. G. Garnier, P. Oelhafen, Adv. Mater. **17**, 574 (2005).
[42]C. Antoniak, J. Lindner, M. Spasova, D. Sudfeld, M. Acet, M. Farle, K. Fauth, U. Wiedwald, H.-G. Boyen, P. Ziemann, F. Wilhelm, and S. Sun, Phys. Rev. Lett. **97**, 117201 (2006).
[43]P. Villars and L. D. Calvet, *Pearson's Handbook of Crystallographic Data for Intermetallic Phases* (American Society for Metals, Metals Park, OH, 1985).
[44]I. Galanakis, M. Alouani, and H. Dreyssé, Phys. Rev. B **62**, 6475 (2000).